

# In-field hyperspectral imaging: An overview on the ground-based applications in agriculture

Alessandro Benelli,<sup>1</sup> Chiara Cevoli,<sup>1,2</sup> Angelo Fabbri<sup>1,2</sup>

<sup>1</sup>Department of Agricultural and Food Sciences, Alma Mater Studiorum, University of Bologna, Cesena (FC);

<sup>2</sup>Interdepartmental Centre for Agri-Food Industrial Research, Alma Mater Studiorum, University of Bologna, Cesena (FC), Italy

## Abstract

The measurement of vegetation indexes that characterise the plants growth, assessing the fruit ripeness or detecting the presence of defects and diseases, is a key factor to gain high quality of fruit or vegetables. Such evaluation can be carried out using both destructive and non destructive techniques. Among non-destructive techniques, hyperspectral imaging (HSI), combining image analysis and visible/near-infrared spectroscopy, looks particularly useful. Many studies have been published concerning the use of hyperspectral cameras in the agronomic and food field, especially in controlled laboratory conditions. Conversely, few studies described the application of HSI technology directly in field, especially involving ground-based systems. Results suggest that this technique could be particularly useful, even if the role of environmental variables has to be considered (e.g., intensity and incidence of solar radiation, wind or the soil in the background). In this paper, recent in-field HSI applications based on ground systems are reviewed.

## Introduction

The hyperspectral imaging (HSI) concept originated from imaging spectrometry (Liu *et al.*, 2015). In the mid-1980s imaging spectrometry, a new Earth remote sensing technique, was develo-

ped at the Jet Propulsion Laboratory (JPL) of the California Institute of Technology in Pasadena, affiliated with the National Aeronautics and Space Administration (NASA). Airborne and spaceborne sensors allowed the identification of surface materials directly and remotely; images of the observed surface were obtained, simultaneously with reflectance values coming from up to 200 contiguous spectral bands in the reflectance spectrum (Goetz *et al.*, 1985).

During the last few decades, numerous imaging and spectroscopic techniques have been developed and implemented by the agricultural and food industries for the evaluation and classification of products based on their intrinsic characteristics and properties (ElMasry and Sun, 2010). In recent years, the integration of imaging and spectroscopy through the development of HSI technology has made it possible to combine their benefits, obtaining results that are difficult to achieve with traditional imaging and spectroscopic technologies (Lu and Park, 2015). As evidence of this, there is a growing interest in research in this field as shown in Figure 1 where the number of papers published in Scopus database (January 2020) in the range of years 2000-2018 on hyperspectral imaging in agricultural and biological sciences and engineering subject areas are reported. The categories 'Cereals', 'Fruits' and 'Vegetables' have been created from the FAO (Food and Agriculture Organisation of the United Nations) Commodity lists (©FAO 1994); in particular, the 'Vegetables' category, was obtained by aggregating the FAO categories vegetables, roots and tubers, pulses and oil bearing crops.

## Operating principles of a hyperspectral camera

A HSI laboratory system (Figure 2) typically consists of a light source, a CCD or CMOS camera with a spectrograph (HSI camera), a translation stage composed by a conveyor belt on which the sample flows, and a computer (ElMasry *et al.*, 2012; Liu *et al.*, 2015).

The operating principle of a HSI camera is comparable to that of an RGB camera: both measure and record the amount of light reflected by the framed object, which reaches the sensor. Both cameras can only partially process the electromagnetic spectrum: the RGB camera sensor measures only three bands of the visible radiation (corresponding to the blue, green and red light), while the HSI camera sensor can measure a few hundred bands within the characteristic wavelength range of the sensor. The amplitude of a few nanometers of the spectral bands determines a high spectral resolution of the HSI sensor (Thomas *et al.*, 2018). To disperse the light into selected wavelengths, optical and electro optical wavelength dispersion devices are used (Liu *et al.*, 2015).

Correspondence: Chiara Cevoli, Department of Agricultural and Food Sciences, Alma Mater Studiorum, University of Bologna, p.zza Goidanich 60, 47521 Cesena (FC), Italy.  
E-mail: chiara.cevoli3@unibo.it

Key words: Hyperspectral; fruits, vegetables; in-field application; prediction; classification.

Received for publication: 12 November 2019.  
Accepted for publication: 15 May 2020.

© Copyright: the Author(s), 2020

Licensee PAGEPress, Italy

Journal of Agricultural Engineering 2020; LI:1030  
doi:10.4081/jae.2020.1030

This article is distributed under the terms of the Creative Commons Attribution Noncommercial License (by-nc 4.0) which permits any non-commercial use, distribution, and reproduction in any medium, provided the original author(s) and source are credited.

### Sensor systems

There are three types of sensor systems (Figure 3): i) ‘whisk-broom’ linear array with a rotating mirror; ii) ‘push-broom’ linear array; iii) area array. The sensor systems with linear arrays include diodes or charge coupled devices that measure the radiance resulting from the object framed. Linear array sensors are often named ‘push-broom’ because their disposition resembles the arrangement of a single line of bristles in a broom (Jensen, 2014). Since the HSI

camera captures only one line of the object framed, a translation stage is used to slide the sample below the lens. In this way a whole scan of the surface of the object can be obtained, then the computer create and display a complete hyperspectral image (Liu *et al.*, 2015). Respect to whisk-broom detectors, push-broom detectors provide a more accurate measurement of the radiant flux reflected by the sample because: i) there are no moving mirrors; and ii) push-broom linear array sensors are able to stay longer on a speci-

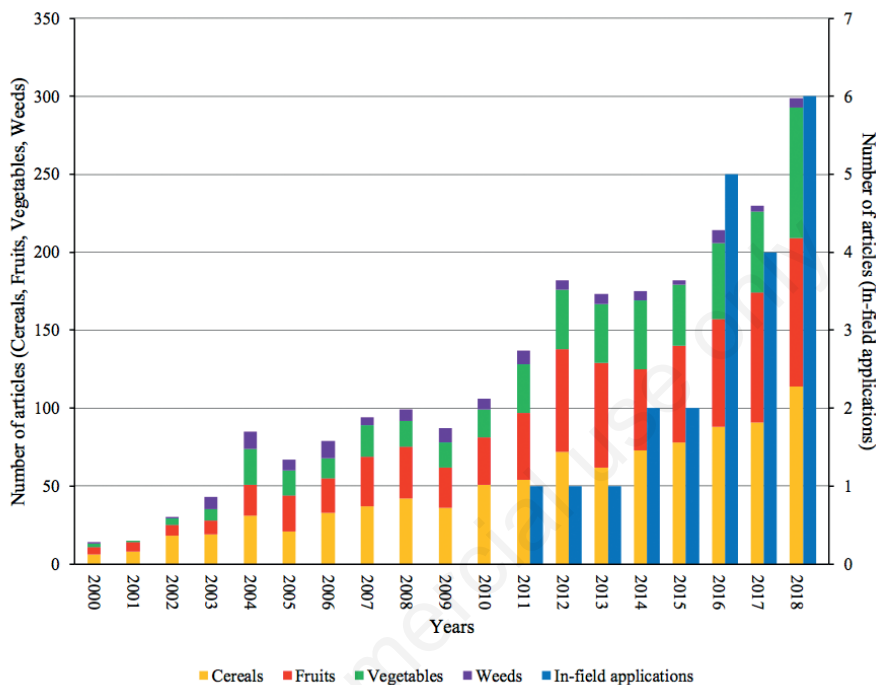


Figure 1. Number of documents published in Scopus database in the range of years 2000-2018 on hyperspectral imaging in agricultural and biological sciences and engineering subject areas.

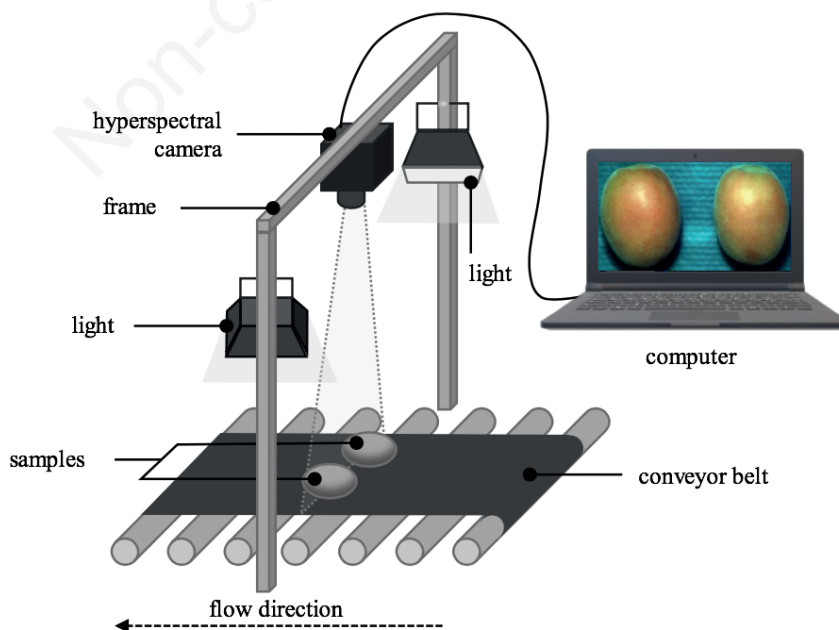


Figure 2. Components of a typical hyperspectral imaging system of the push-broom type.

fic part of the sample (Jensen, 2014). With the area array detector system, hyperspectral images are acquired entirely, one at a time for each spectral band. This system does not require sample or HSI camera movement. A filter, wheel or tunable, is necessary to select different wavelengths during the scanning process (ElMasry *et al.*, 2012). Area array sensor system is more practical in multispectral imaging techniques, where the number of wavelengths selected is limited (Garini *et al.*, 2006).

### The hyperspectral image

In a hyperspectral image, each pixel is characterised by the

information on reflectance, absorbance or transmittance from each spectral band selected. The so-called spectral signature (or spectral profile) can be obtained by summing this information, but it can also be measured through a non-imaging hyperspectral sensor like a spectrometer, losing spatial information (Thomas *et al.*, 2018). HSI, combining spectroscopy and imaging, measures at the same time the spectral signatures and the spatial information from a sample. The HSI data output is a stack of narrow band sub images organised along the reflectance spectrum axis, thus generating a 3-D hypercube (Figure 4). The 3-D cube data (named 'voxel') is characterised by two spatial ( $x, y$ ) and one spectral dimension ( $\lambda$ ) (Mishra *et al.*, 2017).

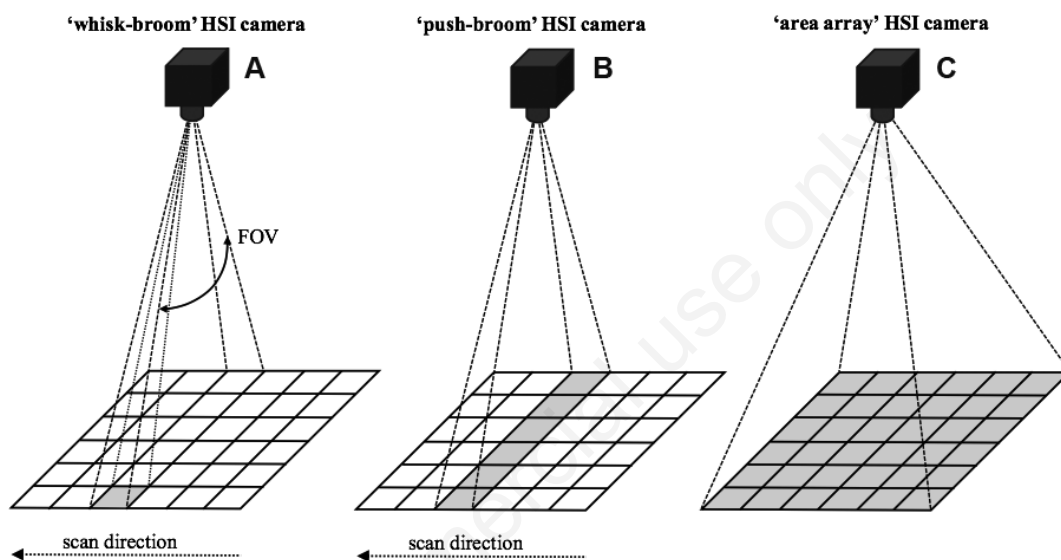


Figure 3. Three types of scanning systems used for multispectral and hyperspectral data collection: A) imaging with a scanning mirror and linear arrays, often referred to as whisk-broom technology; B) hyperspectral imaging with linear arrays, often referred to as push-broom technology; C) digital frame camera based on area arrays. FOV, field of view of the rotating mirror.

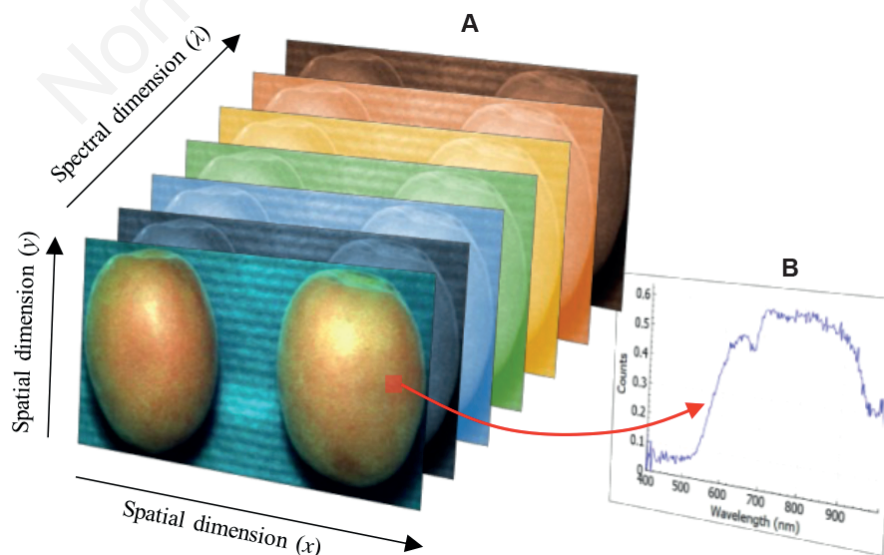


Figure 4. A) Representation of a 3-D hypercube, composed of a stack of sub-images of apricots in contiguous spectral bands; B) Reflectance spectrum of one pixel represented in (A) by a red square.

## Hyperspectral image processing

A typical hyperspectral image processing consists in the following phases: i) calibration and image acquisition; ii) spectral/spatial processing and dimensionality reduction; iii) data elaboration and development of prediction or classification models. Several techniques have been developed to process both the spatial and spectral dimensions of a hyperspectral image. Dimensionality reduction means reduction in data size and extraction of spatial and/or spectral characteristics in a smaller dimensional space. Subsequently, the data can be classified to identify the pixels/spectra useful for the analysis. Regression techniques can also be applied, to estimate a reference parameters in particular, in recent years techniques of chemometric and multivariate analysis have been applied to hyperspectral images (Yoon and Park, 2015).

### Calibration and image acquisition

The calibration of the image acquired in reflectance, absorbance or transmittance mode allows to obtain a corrected image considering a black and a white reference image: the black image can be obtained by placing the cap on the lens of the camera, instead the white image is carried out of a high reflectance material placed inside the framing area (Ma *et al.*, 2019).

### Spectral/spatial processing and dimensionality reduction

Spectrum processing includes pre-processing and extraction of spectral characteristics. The most commonly used techniques are: smoothing methods of random noise from raw data (*e.g.* Savitzky-Golay, moving average, median filter), or spectral pre-processing algorithms to refine the spectral data as the derivatives (Norris-Williams and Savitzky-Golay), multiplicative scatter correction (MSC), standard normal variate (SNV), alignment technique (COW) (Rinnan *et al.*, 2009).

Considering the multivariate models, to avoid problem of multicollinearity, it is useful to make a variable selection. This can improve model performance and model characteristics by identifying and removing useless, noisy and redundant variables (Liu *et al.*, 2014). There are three main variable selection methods: filter methods (information gain and correlation-based feature selection) wrapper methods (learning algorithms, such as beam search, simulated annealing and genetic algorithms) and embedded methods (SMV and decision tree).

Regarding the wavelength selection the most common methods are successive projections algorithm (SPA), stepwise regression (SWR), PLSR and uninformative variable elimination (UVE). Some other algorithms for applications in HSI analysis have been developed recently and exhaustively described by Liu *et al.* (2014).

### Classification and prediction methods

Classification methods include multivariate classification techniques, which comprises: i) unsupervised methods as principal component analysis (PCA), clustering (k-means, Jarvis-Patrick, hierarchical), and convolutional neural networks (CNN); ii) supervised methods as discriminant analysis (linear, quadratic or regularised DA), soft independent modelling class analogies (SIMCA), partial least square discriminant analysis (PLS-DA), support vector machines (SVMs), and the non parametric k-nearest neighbour (kNN) (Ma *et al.*, 2019).

Prediction methods used to estimate the relation between spectral information and reference properties measured on the samples are divided into linear and non linear regression. Linear regression includes multiple linear regression (MLR), principal component

regression (PCR), and linear partial least square regression (PLSR). The most commonly used non linear regression are artificial neural networks (ANN), *e.g.* multilayer perceptron (MLP) or generalised regression neural network (GRNN), SVM and non-linear PLSR (Ma *et al.*, 2019).

## HSI application in the field

Recently, due to the rapid development of computer systems with high data processing capacities and the miniaturization of HSI systems, the opportunity of analysing in real time plants and foods, such as fruits and vegetables directly in the field at ground level, has become more interesting. Satellite based systems or airborne systems (manned or unmanned aerial vehicles, tethered balloons), characterised by low spatial resolution are mainly aimed at the study of the plants canopy and terrestrial vegetation. In addition, ground based systems mounted on agricultural vehicles or fixed platforms have been introduced, due to their high spatial resolution, for the estimation of quality parameters of plants and foods.

In this work, both remotely and directly controlled ground based HSI systems have been considered, which have been used in the field for: i) phenotypic analysis of plants; ii) determination of fruit ripeness, chlorophyll and nitrogen content of plants; iii) detection of fungal diseases, drought stress, weeds, maize stubble in conservative agriculture; and iv) monitoring of canopies under uncontrolled conditions. The search for the papers was carried out on the abstract and citation database 'Scopus' on January 29<sup>th</sup>, 2019: the keywords 'hyperspectral' and 'field' were searched; the search was limited to the subject area 'agri'. Hence, 1069 results were obtained: from the list of results, only the articles that met the purposes of this work were selected (Table 1).

### High-throughput phenotyping

The study of different crop genetic varieties and growth related phenomic effects under different environmental conditions is essential to achieve higher productivity in terms of yield per hectare and sustainable use of natural resources (Underwood *et al.*, 2017). High-throughput phenotyping (HTP) is crucial to improve yield as well as quality and it contributes to a better understanding of plant genomics. However, phenotyping techniques mainly rely on manual measurements and visual inspections. In addition, phenotyping techniques are not developed as well as genotyping techniques in terms of throughput, accuracy, and repeatability. This condition hinders the potential use of plant genotyping data for the development of genotype phenotype maps and for the characterisation of the interactions between genotype and environment (Jiang *et al.*, 2018).

In line with the aforementioned state, Underwood *et al.* (2017) used a high-throughput phenotyping system, designed for row crops composed by a set of grains and legumes. The system described, named *Ladybird UGV*, was based on an unmanned ground vehicle (UGV) that allowed autonomous, high resolution, multi modal sensing and data processing. Hyperspectral data were acquired with a visible to near-infrared (VNIR) push-broom camera (Pika II, Resonon); hyperspectral images were of 648 spatial by 244 spectral pixels, with a spectral resolution of 2 nm in the range from 390.9 to 887.4 nm. Data were compared to those obtained by a hand held sensor named *Greenseeker*. Moderate linear relationships characterised by a  $R^2 = 0.83$  and  $R^2 = 0.72$ , were reported for data acquired in August and September, respectively. *Ladybird UGV* was able to efficiently scan areas of coverage typically used

Table 1. Works cited, in the order in which they are listed in the text, with a brief description of their strengths and weaknesses.

Topics	References	Applications	Strengths	Weaknesses
<b>High-throughput phenotyping</b>				
	Underwood <i>et al.</i> , 2017	Grains, legumes	Adoption of an unmanned ground vehicle, useful in term of labour saving and accuracy. Moderately good results.	Limitation for the tallest plants (faba beans). Potential for crop damage.
	Jiang <i>et al.</i> , 2018	Cotton	Multi-instrumental system. Moderately good results.	The implementation of a cover reduced the amount of incident sunlight, requiring the use of artificial lights.
	Gutiérrez <i>et al.</i> , 2018	Grapevine	Real time, on the go HSI approach. Good prediction performance.	Nothing to report.
	Deery <i>et al.</i> , 2014	Wheat	Multi-instrumental system.	Requires a high degree of expertise.
<b>Fruit ripening</b>				
	Wendel <i>et al.</i> , 2018	Mango	Adoption of an unmanned ground vehicle. Dry matter prediction of on-the-tree mangoes is possible and repeatable.	The geometry of the trees, the shadows of the fruits and the variation in the intensity and angle of the solar radiation affected the result.
<b>Chlorophyll content</b>				
	Wang <i>et al.</i> , 2018	Rice canopy	The spectral purification procedure developed contributes to reduce the background impact. Moderately good results.	The method lacks automation.
	Wu <i>et al.</i> , 2016	Wheat leaves and canopy	Good results from single wheat plant leaves	Low precision of canopy spectral data, due to soil in the background.
	Jay <i>et al.</i> , 2017	Sugar beet canopy	Good performances achieved with an optimised vegetation index.	Results affected by a great variability of leaf orientation and lighting conditions.
	Al Makkessi <i>et al.</i> , 2017	Durum wheat canopy	Development of a light propagation model based on 3D models. Acceptable nitrogen content prediction.	Multiple scattering effects mainly affect the lower leaves, which cannot be discarded due to a significant loss of information.
	Malenovsky <i>et al.</i> , 2015	East Antarctic dominant mosses	Good chlorophyll a and b, and leaf density estimation.	The prediction of the turf water content was influenced by the selection of the near infrared spectral region, which does not include wavelengths with adequate water absorption.
<b>Nitrogen content</b>				
	Onoyama <i>et al.</i> , 2015	Rice plant	Good results applying the growing degree-day parameter, related to air temperature, to predict nitrogen content.	The wind has made some of the captured images unusable.
	Onoyama <i>et al.</i> , 2018	Brown rice	Good prediction performance adopting 4 regions of interest models.	Exception on good prediction performance for the dark area model. Strong wind affected the capture of two images.
	Vigneau <i>et al.</i> , 2011	Wheat leaves	Complications introduced by variable solar lighting and plant architecture were considered. Good prediction performance of leaf nitrogen content.	Models are dataset dependent, probably due to low sample number and growing conditions, in particular with regard to the plant nitrogen supply.
	Whetton <i>et al.</i> , 2018	Wheat, barley	Performance was better in wheat than in barley.	Use of an external light source.
	Zhao <i>et al.</i> , 2016	Winter wheat	Able to follow the vertical features of the infestation.	The method lacks automation.
<b>Drought stress detection</b>				
	Römer <i>et al.</i> , 2012	Barley, corn	Corn: clear detection of clusters, determined by two irrigation and nitrogen availability regimes.	Barley: the experiment was conducted inside a rain out shelter.
<b>Weeds detection and management</b>				
	Pantazi <i>et al.</i> , 2016	Corn	Use of an autonomous platform and information system. Excellent crop recognition performance, using one class classifications constructed on neural networks.	One class classifiers based on support vector machine and autoencoders have failed, in most cases, to yield acceptable results.
	Herrmann <i>et al.</i> , 2013	Wheat	Detection of four categories, with a good accuracy: weeds (2), wheat and soil.	In most of the cases, shaded classes produced less user's and producer's accuracies than the respective sunlit class
	Huang <i>et al.</i> , 2016	Palmer amaranth, Italian ryegrass, soybeans	On-the-go HSI system. Excellent accuracy obtained on glyphosate resistant and sensitive weeds differentiation.	Wind interference and sensor overheating due to intense solar irradiation had affected the experiment.
	Reddy <i>et al.</i> , 2014	Palmer amaranth	Excellent validation accuracy of the field model classification, able to differentiate between glyphosate resistant and sensitive palmer amaranth plants.	Nothing to report.
<b>No tillage in conservative agriculture</b>				
	Chen <i>et al.</i> , 2017	Corn stubble	Good capacity to detect corn stubble, useful in corn wheat rotation systems in case of no tillage sowing.	The study is limited to the selection of optimal wavelengths by means of principal component analysis to optimise image segmentation.
<b>Canopy monitoring under uncontrolled conditions</b>				
	Rodriguez-Moreno <i>et al.</i> , 2016	Wheat	The error in estimation of crop reflectance was compatible with a proper agronomic interpretation of the images using thresholds, linear functions or combination of both.	The main problem observed is not the accuracy of the measurements, but the precision.

in real world scientific phenotyping studies. This way of operating was faster than optimised traditional manual measurement, and it was able to generate highly repeatable and accurate data (Underwood *et al.*, 2017).

The field-based high-throughput phenotyping (FB-HTP) system developed by Jiang *et al.* (2018), named *GPhenoVision*, consisted of a high-clearance tractor with imaging, environmental and GPS sensors; it was evaluated by field scan of 23 cotton genotypes, to quantify canopy growth and development. Imaging sensors consisted of a conventional RGB-D, a thermal and a hyperspectral camera (MRC-923-001, Middleton Spectral Vision, Middleton, WI, USA). HS camera has a spectral range of 400-1000 nm, an image resolution of 640 (spatial)  $\times$  236 (spectral), and a nominal spectral resolution of 2.7 nm. About imaging tests, to reduce the intensity of sunlight and wind effects a cover was adopted, but with this configuration the intensity of the signal recorded by the hyperspectral camera was low due to the reduced amount of incident light. Finally, regarding the hyperspectral camera, three calibration lamps were used to obtain a more accurate regression. In the present study, six phenotypic traits were extracted: plant height, width in-row (WIR), width across-row (WAR), projected leaf area (PLA), canopy volume (CV) and canopy expansion (Tc-Ta). The considered traits had a moderate correlation ( $r = 0.54-0.74$ ). These results suggested that a quantitative genetic analysis could be conducted and yield prediction models could be developed (Jiang *et al.*, 2018).

Phenotyping of grapevine varieties is important both for producers and for the wine industry (Gutiérrez *et al.*, 2018). Gutiérrez *et al.* (2018) classified a high number of grapevine varieties under field condition and natural illumination using a hyperspectral camera system (Pika L VNIR hyperspectral imaging camera, Resonon, Inc., Bozeman, MA, USA) mounted on an all-terrain vehicle (ATV). The horizontal movement of the ATV regulated the scanning of the push-broom type line scan hyperspectral camera. Data were processed by using SVM and artificial neural networks (multilayer perceptrons, MLP) testing several spectra pre-processing methods. Recall (the ratio of the number of correctly classified samples to the total number of testing samples), F1 value [ $2 \times (\text{precision} \times \text{recall}) / (\text{precision} + \text{recall})$ ] and AUC (area under the receiver operating characteristic curve) were used as performance statistics. The prediction performance of SVM respect to individual varieties resulted in a range from 0.83 (recall) to 0.93 (AUC), while for MLP between 0.95 (recall and F1 score) and 0.99 (recall and F1 score), showing a low variability, in particular the AUC values (Gutiérrez *et al.*, 2018).

To keep up with the development of genomic technologies, fast and accurate crop phenotyping methods are required, in order to meet expected growing demand for food and fibre in the future (Deery *et al.*, 2014). In this perspective, Deery *et al.* (2014) described the development of a ground based proximal remote sensing buggy named 'Phenomobile', implementing these sensors: three LiDAR, four RGB stereo cameras, a thermal infra red camera, three infra red thermometers and a hyperspectral subsystem. The latter is composed by a full range spectroradiometer (Fieldspec 3, ASD Inc., Boulder, CO, USA) and a Vis-NIR hyperspectral line scanner camera (Micro-Hyperspec, Headwall Photonics Inc., Fitchburg, MA, USA). Sensors were mounted on a height adjustable bar (max 3 m from the ground). The frame of the *Phenomobile* was designed to traverse a mature wheat crop (1.2 m ground clearance and 1.8 m width) without coming into contact with the canopy, at a typical operating speed of 1  $\text{ms}^{-1}$ . Moreover, *Phenomobile* presented a Real Time Kinematic GPS characterised by about 2 cm resolution, and a removable light bank (Deery *et al.*, 2014).

## Fruit ripening

Fruit should ripen on the tree, to allow accumulation of sugars and starch getting the best harvesting conditions. Fruits would have to reach on-tree physiological maturity, finding a balance between on-tree ripening and characteristics required for transport and storage. Hyperspectral imaging systems implementation directly in-field can help farmers to optimise harvest time, evaluating the grade of ripening of fruits (Wendel *et al.*, 2018). In the study of Wendel *et al.* (2018), a hyperspectral camera (Resonon Pika II visible to near infrared (VNIR) line scanning hyperspectral camera, with a spectral range of 411.3-867.0 nm), a LIDAR sensor and a navigation system mounted on a ground vehicle contributed to carry out the measure of dry matter (DM) of mango to evaluate maturity. DM resulted from measures performed by a hand-held NIR spectrometer of harvested and on-tree fruit. These data were elaborated by using PLSR and CNN. Considering the cross-validation data set,  $R^2 = 0.64$  and  $\text{RMSE} = 1.08\%w/w$  was achieved by CNN in fruit on tree, while  $R^2 = 0.58$  and  $\text{RMSE} = 1.17\%w/w$  was achieved by PLS. Moreover, PLSDA and a CNN were compared to discriminate non mango pixels from mango pixels, obtaining good classification performance (mean F1 score  $> 0.97$ ). The described system permitted to predict the maturity of fruits at a distance from trees, but presented difficulties due to the geometry of the trees, the shadows of the fruits and the variation of the intensity and angle of solar radiation (Wendel *et al.*, 2018).

## Chlorophyll content

Determining chlorophyll quantitative variation during plant growth can be useful to monitor the physiological state of the plant, to better understand the growing status and consequently to estimate the yield of the plant (Jay *et al.*, 2017).

Wang *et al.* (2018) captured rice canopy images with an imaging spectrometer (Cubert S185 Imaging Spectrometer, with a 4 nm of spectral resolution and a spectral range of 450-950 nm). Rice leaf hyperspectral images were obtained, in order to retrieve chlorophyll content from refined leaf spectra resulting from 58 rice canopies and to estimate the yield of paddy rice. Vegetation indices extracted from those hyperspectral data were correlated with crop chlorophyll density measured with a SPAD meter (soil plant analysis development chlorophyll meter), with the aim to estimate leaf pigment content. Three vegetation indices with the highest correlation were selected and used: photochemical reflectance index (PRI), structural independent pigment index (SIPI) and green normalised difference vegetation index (GNDVI). A PLSR was used, obtaining in cross validation  $R^2 = 0.703$  before purification, and  $R^2 = 0.753$  after purification. A commonly used field portable spectroradiometer can only obtain point spectral information. However, the device is not able to obtain spectral and image information at the same time. Usually, canopy spectral data resulting from a spectroradiometer are the average of spectra collected in a specific area and are affected by the weaker part of the plant, which is located under the foliage, and by the environment (Wang *et al.*, 2018).

Wu *et al.* (2016) analysed canopy and single wheat plant leaves at seedling stage using a spectroradiometer and a planar array visible near infrared hyperspectral camera (VNIR hyperspectral MS4100 high resolution 3 CCD camera, Redlake Inc.) to establish prediction models to monitor plant growth. Data obtained by the two instruments were correlated to plant growth measured factors (chlorophyll SPAD value, nitrogen and water content, dry matter). The hyperspectral camera adopted is more portable, with a higher acquisition rate and without the necessity to move the ground support mounted on a rail, respect to a push-broom hyperspectral

camera. Due to the soil in the background, both the spectral data of canopy obtained with the two instruments were characterised by low precision. Instead, spectral data from single wheat plant leaves obtained with the hyperspectral camera were more detailed, gaining a correlation coefficient  $r$  of 0.8836, 0.8520 (PLSR) for chlorophyll SPAD and nitrogen content, respectively (Wu *et al.*, 2016).

Jay *et al.* (2017) studied methods based on reflectance observations for non-destructive leaf chlorophyll content ( $C_{ab}$ ) estimation at field level in sugar beet canopies. It was adopted a push-broom hyperspectral camera (HySpex VNIR 1600, Norsk Elektro Optikk, Norway) in the 400-1000 nm range, with high spatial resolution (millimetre to centimetre) mounted on a ground-based platform. The push-broom camera was positioned at 1.1 m above the ground and vertically oriented. At this scale, soil reflectance and the shape of canopy structure interact with the scattering properties related to leaf, producing canopy reflectance. Effects of canopy structure and leaf architecture (leaf orientation and spatial distribution) should be carefully straighten out when relating remote sensing observations to foliar biochemistry. The best performances were achieved with an optimised vegetation index named 'modified normalise difference',  $mND[\lambda_1, \lambda_2]$ , defined as  $(R_{\lambda_{ref}} - R_{\lambda_1}) / (R_{\lambda_{ref}} + R_{\lambda_2})$ , using a blue reference spectral band  $\lambda_{ref} = 440$  nm ( $R_{\lambda}$  refers to the reflectance at the given wavelength). Data were computed considering the average reflectance spectra related to the 50% brightest green pixels, with a spatial resolution equal to 3.5 cm.  $mND_{blue}[728, 850]$  was correlated with  $C_{ab}$  using a linear regression model, obtaining  $R^2 = 0.83$  and  $RMSEP = 2.45 \mu g cm^{-2}$  (Jay *et al.*, 2017).

Leaf radiance variation is strongly induced by the great variability of leaf orientation and lighting conditions (Jay *et al.*, 2017). At this regard, Al Makdessi *et al.* (2017) implemented the 'Caribu' light propagation model on 3D models of durum wheat canopy, trying to obtain a picture of the spectra variability induced by the leafy architecture. Spectra were acquired in various phases on leaves completely expanded using a field spectrometer [FieldSpec, Analytical Spectral Devices, Inc. (ASD), Boulder, Colorado, USA] with a leaf clip. A PCA was performed to analyse the distribution of resulting simulated spectra in the spectral feature space. Finally, the performance of PLSR in predicting leaf nitrogen content (LNC) was evaluated. At the plant level, considering only the leaves on the top of the plant, it revealed an acceptable nitrogen content prediction, with an error about 0.5% of dry matter (Al Makdessi *et al.*, 2017).

Near distance imaging spectroscopy was used by Malenovský *et al.* (2015) to evaluate spatial distribution of three East Antarctic dominant mosses (*Bryum pseudotriquetrum*, *Ceratodon purpureus* and *Schistidium antarctici*), due to the reduction of liquid water availability caused by latest environmental changes. Three quantitative stress indicators were used: turf chlorophyll a and b ( $C_{ab}$ ), water content (TWC) and leaf density (LD). Reflectance was measured in the laboratory and outdoors in both poor and abundant water conditions. Field measurements were performed by an imaging push-broom type spectroradiometer (Headwall Photonics Micro-Hyperspec VNIR scanner, Headwall Inc., Fitchburg, MA, USA) mounted to a geodetic tripod on a rotation and tilt platform. In the spectral range of 496-898 nm, ten bands were selected, three in the visible (496-710 nm) and seven in the near infrared (710-848 nm). The best results were obtained estimating the reflectance continuum removal (CR) transformation of  $C_{ab}$  applying SVR on reference and remotely sensed spectra trained with all the three species of mosses together and considering the wavelengths between 648-719 nm, specific for chlorophyll absorption [ $RMSE = 238.3 nmol g^{-1} DW$  (dry weight) and  $R^2 = 0.54$ ]. The best LD estimation was

achieved on *S. antarctici*, adopting SRV trained with the reflectance between 708 and 782 nm ( $RMSE = 1.8 leaves mm^{-1}$ ,  $R^2 = 0.55$ ) (Malenovský *et al.*, 2015).

## Nitrogen content

Nitrogen nutrition index (NNI) is an expensive, laborious and destructive method to assess plant nitrogen status during plant cycle. Since nitrogen is an essential nutrient and the main limiting factor of plant growth, many new non-destructive techniques have been proposed to replace NNI, such as hyperspectral imaging (Vigneau *et al.*, 2011).

Onoyama *et al.* (2015) developed a ground-based hyperspectral imaging system to estimate rice plants nitrogen content at the panicle initiation stage. In rice cultivation, nitrogen is applied in the form of topdressing in the early stages of panicle development, in order to increase the yield in terms of rice grains. The hyperspectral imaging system adopted consists of a prism-grating-prism (PGP) component and a monochrome camera (ImSpector QE V10E; Specim, Oulu, Finland), with a nominal spectral range between 400 and 1000 nm and a 5 nm nominal spectral resolution. A planetary gearbox rotational stage rotated the camera with the aid of a motor, for push-broom type line scan. Three PLSR models were tested, including both the reflectance and the growing degree days (GDD), to explain the differences in growing temperature conditions over a 3-year period (2008, 2009, and 2010): 1-year model, 2-year model and 2-year model based on GDD. GDD represents a meteorological condition frequently used to describe the timing of biological processes: it was calculated based on air temperature measurements. In order to determine the adaptability of the PLSR models to test data collected in different years, a mutual estimation of the values for the other years was calculated. In 1-year model, the RMSE and relative error (RE) values of the mutual estimation resulted much higher respect to the values of the validation of the same 1-year model (RMSE from 0.49 to 3.95  $g/m^2$  and RE from 8 to 85% in mutual estimation, RMSE from 0.48 to 0.65  $g/m^2$  and RE from 7 to 15% in validation), because of underestimation and overestimation. Similar results were obtained by applying the 2-year model, without significant differences in accuracy respect to the 1-year model (mutual estimation RMSE from 1.29 to 3.32  $g/m^2$  and RE from 21 to 43%). The introduction of GDD in the 2-year model (third model) resulted in a decrease in mutual estimation RMSE and RE values (RMSE from 0.55 to 0.95  $g/m^2$  and RE from 8.2 to 13%), proving its usefulness for predicting the nitrogen content. Ultimately, it has been shown that the combination of reflectance and temperature data could be used to construct a model that explains the changes in growth conditions of rice plants at the heading stage (Onoyama *et al.*, 2015).

In brown rice production, it is important to consider grain quality as well as grain yield. A ground-based hyperspectral imaging system (ImSpector QE V10E, Specim, Oulu, Finland) with a nominal spectral range from 400 to 1000 nm, and a nominal spectral resolution of 5 nm, was used for the estimation of protein content before harvest. Protein content is related to rice taste quality; furthermore, it is also useful for establishing the application plan of the amount of basal and top dressing fertiliser for the following year. The use of a spatial scanning hyperspectral camera allowed to obtain three dimensional data. In spatial scanning, spatial spectral three dimensional images can be collected line by line through rotational movement of the camera powered by a motor. Instead, one dimensional data, deriving from a common spectroradiometer and represented by the reflectance of the analysed target, also include unwanted parts, such as soil background. The reflectance of five regions of interest (ROI-I: target area; ROI-II: dark area;

ROI-III: canopy area; ROI-IV: leaf area; ROI-V: ear area) were related with protein content according to PLSR analysis.  $R^2$  and RMSE prediction values were similar for each model, with  $R^2$  values between 0.83 and 0.86, and RMSE between 0.27 and 0.30%, but with the exception of the dark area model, where  $R^2 = 0.76$  and  $RMSE = 0.35\%$ . No significant differences in the magnitude of the estimation error between all models were observed. (Onoyama *et al.*, 2018).

Vigneau *et al.* (2011) developed a system composed by a push-broom CCD camera (HySpex VNIR 1600-160, Norsk Elektro Optikk, Norway) installed on a tractor mounted motorised rail. The camera operated in the spectral range between 400 and 1000 nm, with a spectral resolution of 3.7 nm (160 wavelength bands). Close range hyperspectral images acquired were used to evaluate leaf nitrogen content in wheat. The study also considered in-field complications introduced by variable solar lighting and plant architecture, such as illumination level variation induced by leaf inclination and specular reflection. Reflectance pre-processing and correction process led to the same quality of results obtained in laboratory. A PLSR model considering nitrogen concentration and reflectance spectra of single leaves was developed; it was obtained by grouping two datasets, related to plants grown in pots in greenhouse or in field conditions. The model predicted leaf nitrogen content for the two growing conditions, with  $R^2 = 0.875$  (test step), and standard error of prediction corrected of the bias ( $SEP_c$ ) = 0.496% DM (Vigneau *et al.*, 2011).

In summary, hyperspectral images produced spatial nitrogen cartographies, and it was possible to monitor nitrogen dynamics at leaf level. Consequently, these data could be implemented in growing models or nitrogen remobilisation models (Vigneau *et al.*, 2011).

### Fungal diseases detection

Cereal production can be compromised by the presence of in-field fungal diseases. Due to their spatial variability, it is necessary to acquire high spatial resolution data to perform a detailed site specific control of the diseases (Whetton *et al.*, 2018).

Whetton *et al.* (2018) measured two fungal diseases with a mobile measurement system in four fields of wheat and barley: yellow rust (determined by *Puccinia striiformis*), one of the most detrimental foliar disease of wheat in cool climates, and fusarium head blight (*Fusarium graminearum*), producing mycotoxins in the grain. Such online system consisted of a push-broom hyperspectral camera (HS spectral camera model from Gilden Photonics Ltd., UK) attached to a tractor, with an external light source; the camera works in the spectral range of 400-1000 nm. The percentage of coverage of the diseases was assessed using two methods, in-field visual assessment (IVA) and photo interpretation assessment (PIA) on the basis of a 100-point grid superimposed on RGB images. The spectral data were analysed by PLSR with leave-one-out cross-validation. Measurements of yellow rust and fusarium head blight were similarly accurate, while performance was better in wheat than in barley. PIA analysis resulted more accurate than IVA for fusarium. Considering PIA analysis, residual prediction deviation (RPD) value was 2.27 and  $R^2$  value was 0.82 for wheat, while RPD was 1.56 and  $R^2$  was 0.61 for barley. On the contrary, IVA analysis was more accurate than PIA in the yellow rust. In barley RPD and  $R^2$  values were 1.67 and 0.72, while in wheat they were 2.19 and 0.78 respectively (Whetton *et al.*, 2018).

The yield and quality of winter wheat grains can also be seriously compromised by yellow rust. For this purpose, a hyperspectral imaging spectrometer (ImSpector V10E, Specim, Spectral Imaging Ltd., Finland) was used to accurately assess wheat yellow

rust. The instrument works in the wavelength range between 400 and 1000 nm, with a spectral resolution of 2.8 nm. This ground-based imaging spectrometer system collected images in a push-broom manner. It consisted of a camera, a spectrograph, a mount zoom lens, and a mirror scanner: the system generates a hyperspectral data cube, which simultaneously collected spectral and imaging characteristics of pure yellow rust spores. Three flag leaves (F-1, F-2 and F-3: F = flag leaf) were randomly collected from the inoculated and normal wheat fields. Six region of interest (ROI) from the tip to the bottom of the three samples were analysed, finding a relation between the general trend of chlorophyll content (F-1 > F-2 > F-3) and the averaged hyperspectral reflectance measured; reflectance values gradually increased (F-1 > F-2 > F-3) in the visible region selected (520-720 nm) and decreased (F-1 < F-2 < F-3) in the NIR region (730-1000 nm) (Zhao *et al.*, 2016). Compared to a conventional non-imaging spectrometer, a hyperspectral imaging system is particularly useful to detect the disease development along the leaf layers, following the vertical features of the infestation, in the appropriate growth phases considered. Furthermore, spectral and image data can be collected at once, regularly and automatically. In this way, it may be decided to spray the fungicides, especially in the initial stages of the infestation (Zhao *et al.*, 2016).

### Drought stress detection

Hyperspectral imaging sensors were adopted to evaluate early water stress: i) on barley (SOC-700, Surface Optics Corp., San Diego, CA, USA) in controlled drought conditions inside a rain-out shelter; and ii) on corn (PS V10E, Spectral Imaging Ltd, Oulu, Finland,) directly in the field, in order to check if the method is applicable both in controlled conditions and in the field. The linear push-broom hyperspectral camera used on corn (PS V10E) is characterised by a spectral resolution of 2.8 nm in the range between 400 and 1000 nm (Römer *et al.*, 2012).

A deterministic method to analyse data was introduced, named simplex volume maximisation (SiVM). The applicability of this matrix factorization technique was tested for the first time in plant sciences; it was also a new approach for unsupervised learning of relevant patterns. With regard to the corn experiment, plants were grown in an experimental field with two different irrigation regimes (rain-fed and full irrigation) and nitrogen availability. In addition, several vegetation indices (VIs), including the normalised difference vegetation index (NDVI) and the photochemical reflectance index (PRI), were tested. The results have shown that SiVM divided the four treatments into three well separated clusters. Regarding the VIs, the PRI detected a difference in nutrient treatment, but was not able to detect water, while the NDVI detected drought, but was not able to detect nutrient treatment. A combined assessment with PRI and NDVI was effective in successfully detecting all four clusters. In summary, SiVM has given considerable better results than the use of a combination of vegetation indices. In the corn plots, although the effect of the treatments on the foliar and canopy traits was reduced, SiVM managed to separate them (Römer *et al.*, 2012).

### Weeds detection and management

Ground-based remote sensing techniques (GBRST) provide interesting utilisations for precision agriculture (Huang *et al.*, 2016). Crop production and yield are influenced by the presence of weeds, and the use of herbicides implies high costs and environmental impact. A method based on machine learning, developed by Pantazi *et al.* (2016), was used to discriminate between corn and

weed species considering differences in spectral reflectance; Herrmann *et al.* (2013) developed a hyperspectral imaging (HSI) system to separate weeds from wheat.

Pantazi *et al.* (2016) obtained hyperspectral images from a HSI system (ImSpector V9, Specim, Spectral Imaging Ltd., Oulu, Finland) mounted on a robotic platform (autonomous platform and information system). This HSI system consisted of a prism-grating-prism (PGP) line spectrograph with a spectral resolution reduced to 19 nm and a spectral range between 435 and 834 nm, integrated with a monochromatic camera. Subsequently, four discrimination wavebands were selected using a stepwise variable selection. Four novelty detection classifiers have been implemented, based on one-class classification constructed on neural networks: SVM, autoencoder, mixtures of Gaussians (MOG) and self-organising maps (SOM). The best results were obtained using the SOM and MOG classifiers. The crop recognition performance was 100% for both MOG and SOM classifiers. For the MOG classifier, the correct recognition of the different weed species ranged from 31% to 98%. For the SOM classifier, the correct recognition rate ranged between 53% and 94% (Pantazi *et al.*, 2016).

Herrmann *et al.* (2013) adopted a ground-level image spectroscopy, characterised by high resolution at spatial and spectral level, in order to increase efficiency in weed control in wheat fields. Hyperspectral images were obtained by a push-broom type hyperspectral camera (ImSpector V10E, Specim, Spectral Imaging Ltd., Oulu, Finland) mounted on a tripod. The hyperspectral camera works in the NIR and visible regions, with a spectral range between 400 and 1000 nm and a spectral resolution of 2.8 nm. PLSDA was applied to classify four categories and not for specific species of weeds: i) category BLW (broadleaf weeds) included the species *Chenopodium*, *Mallow* and potato; ii) category GW (grass weeds) included *Lolium rigidum* and *Hordeum plaucum*, the third and fourth categories corresponded to iii) wheat and iv) soil. The models developed considered a combination of some or all of the categories, even if the spectra were obtained from sunlight pixels and shaded pixels. The best model was the one that included the 4 categories described, but without discriminating between sunlight and shaded pixels. This model was chosen by comparing the cross-validation confusion matrices in terms of variances and the Cohen's Kappa values: K was 0.79 and the total accuracy was 85%. In addition, it was found that the red edge is the most important spectral region for vegetation classes through the application of the variable importance in projection method. The authors concluded that due to high spectral and spatial resolutions it was possible to obtain a separation between wheat and weeds on the basis of their spectral data. This approach could lead to a reduction in herbicides needing and consequently to an improvement both from an environmental and economic point of view so, without diminishing weed control efficiency, to a benefit for farmers and consumers. In addition, reduction of herbicides amount can limit the development of weed resistance to herbicides (Herrmann *et al.*, 2013).

Regarding weed management, it is also useful to detect lesions caused to crops by the spread of a herbicide in the fields next to the one treated, as in the case of dicamba, or the differentiation between resistance and sensitivity to herbicides in weeds, in the case of glyphosate (Huang *et al.*, 2016). For this purpose, Huang *et al.* (2016) adopted three instruments: i) a handheld spectroradiometer, to quickly measure in-field plant canopy spectra; ii) a push-broom hyperspectral camera (Resonon Pika II, Resonon, Bozeman, MT) with two lamps as a light source for laboratory use, and iii) an on the go hyperspectral camera, the same used in laboratory, mounted to a 3 point hitch installed on the back of a standard tractor, for

in-field study of plant canopy. The hyperspectral camera works in the range between 400 and 900 nm, providing 240 wavelength bands. The in-field hyperspectral system allowed obtaining an over 90% accuracy on glyphosate-resistant (GR) and glyphosate-sensitive (GS) weeds differentiation. Wind interference on the linear scanning sensor and sensor overheating due to intense solar irradiation had affected in-field experiment. According to this, the authors reported the needing to remove data artefacts and minimize environmental and systemic interference (Huang *et al.*, 2016).

Reddy *et al.* (2014) reported that some populations of Palmer amaranth (*Amaranthus palmeri* S. Wats.), weeds present in the southern United States, have developed resistance to glyphosate. Spectra of GR and GS plants were recorded, and the potential of hyperspectral sensors to differentiate GR from GS plants were explored. The study was conducted both in greenhouse and in the field. In greenhouse, a push-broom type hyperspectral camera (Resonon Pika II, Resonon, Bozeman, MT) was mounted on a stand, and two incandescent light bulbs were used as artificial light source. In the field, the same hyperspectral camera was mounted on a three-point hitch, with the capacity to move horizontally and vertically, and with the sun acting as a natural source of light; in turn, the tripod was installed on a tractor. Spectral data were randomly assigned to training and testing groups, and sensitive hyperspectral bands were selected using a forward selection algorithm. Fisher's linear discriminant analysis (FLDA) was used to reduce the dimensionality of the sensitive bands related to the plant set and the maximum likelihood (ML) to classify the plants. Finally, amaranth plants were classified with confusion matrix with predictive accuracy, through leave-one-out validation. Authors observed that four distinct regions of the spectrum (400-500 nm, 650-690 nm, 730-740 nm and 800-900 nm) were able to separate GR from GS plants. Considering fourteen wavebands within or close to these four spectral regions, the validation accuracy of the field model classification was 96.4% and was comparable with that of the greenhouse model, which was 93.8%. In conclusion, it can be stated that hyperspectral imaging has a potential application to differentiate between GR and GS Palmer amaranth plants, without subjecting them to a glyphosate treatment. For this reason, the technique described could have future implications for glyphosate resistance management (Reddy *et al.*, 2014).

### No tillage in conservative agriculture

Among basic principles of conservation agriculture (CA) are included zero tillage and permanent soil organic cover, which contribute decreasing soil degradation and increasing fertility (Chen *et al.*, 2017; FAO, 2017).

Chen *et al.* (2017) reported that in North China Plain, where annual maize wheat rotation is commonly implemented, the standing maize stubble, and consequently their extensive root system, stays in the field. These materials can hardly decompose during the short period between maize harvesting and wheat sowing, causing the block of the next no till sowing. To address the above problem, a vision-based guide was developed. It consisted of a HSI system mounted on a pedestal. The HSI system comprised a spectrograph (1003B-20001 Micro-Hyperspec VNIR A-Series, Headwall Photonics Inc.) with a spectral range between 347.4 and 952.8 nm (VIR-NIR) and a spectral resolution of 1.846 nm, thus providing 329 wavebands; the spectrograph was coupled to a CCD camera, a zoom lens and a tilt-shift motion control system (PTU-D48E, FLIR). The HSI system was positioned forward during wheat sowing to avoid the standing maize stubble and consequently the underground root system. From the hyperspectral images of the standing maize stubble left in the field, three images with optimal

wavebands (484, 561 and 580 nm) were selected by PCA. The three selected images were then enhanced by means of median filter, Sobel filter, Gaussian lowpass filter, band fusion method. In summary, the enhanced images demonstrated the capacity of the selected optimal wavebands to detect maize stubble (Chen *et al.*, 2017).

### Canopy monitoring under uncontrolled conditions

Rodríguez-Moreno *et al.* (2016) tested the quality of spectral images acquired under uncontrolled and consequently not optimal circumstances.

Multispectral images were acquired from a multispectral camera (DuncanTech MS3100 camera, Auburn, CA, USA) mounted on an on-ground platform without a system to control: i) lighting; ii) the geometry existing between the sun, the target and the sensor; and iii) interferences (dew, dust, *etc.*). Multispectral images were compared with spectral data obtained from a field radiometer and with hyperspectral images acquired by an airborne hyperspectral sensor. In this way, it was possible to measure the error occurring in crop reflectance as well as to evaluate the consequences of the uncontrolled conditions. It was observed that the error in estimation of crop reflectance was compatible with a proper agronomic interpretation of the images using thresholds, linear functions or combination of both (Rodríguez-Moreno *et al.*, 2016).

### Conclusions

Hyperspectral imaging technology for non-destructive analysis by means of high resolution proximal sensing of plants directly in the field is currently not widely adopted, but promising. HSI can be considered in the field of precision agriculture: it is useful for high-throughput phenotyping, for determining the 'harvest maturity' of fruit, for monitoring the physiological state of the plant, parasite attacks, weeds, and consequently for the estimation of the production yield. Some factors complicate the analysis, such as variations in the level of intensity of sunlight, the angle of inclination of the incident solar radiation, overheating of the sensor due to intense solar radiation, the plant architecture that includes the inclination of the leaves and specular reflection, the wind.

Future researches should focus on studying solutions to these problems and on automating the process of acquiring and processing the enormous amount of data obtained from the analysis.

### References

- Al Makdessi N., Jean P.A., Ecartot M., Gorretta N., Rabatel G., Roumet P. 2017. How plant structure impacts the biochemical leaf traits assessment from in-field hyperspectral images: A simulation study based on light propagation modeling in 3D virtual wheat scenes. *F. Crop. Res.* 205: 95-105.
- Chen W., Li H., Niu Q., Hongnan H. 2017. Hyperspectral image segmentation for maize stubble in no-till field. p 6 in 2017 ASABE Annual International Meeting. American Society of Agricultural and Biological Engineers, USA.
- Deery D., Jimenez-Berni J., Jones H., Sirault X., Furbank R. 2014. Proximal remote sensing buggies and potential applications for field-based phenotyping. *Agronomy* 4: 349-79.
- ElMasry G., Kamruzzaman M., Sun D.W., Allen P. 2012. Principles and applications of hyperspectral imaging in quality evaluation of agro-food products: a review. *Crit. Rev. Food Sci. Nutr.* 52:999-1023.
- ElMasry G., Sun D.W. 2010. Principles of hyperspectral imaging technology, Chapter 1. In: Wen S.-D. (Ed.), *Hyperspectral Imaging for Food Quality Analysis and Control*. Academic Press, pp. 3-43.
- FAO, 2017. Conservation Agriculture - Revised version. AG Dept factsheets.
- Garini Y., Young I.T., McNamara G. 2006. Spectral imaging: Principles and applications. *Cytom. Part A* 69A:735-47.
- Goetz A., Vane G., Solomon J., Rock B. 1985. Imaging spectrometry for earth remote sensing. *Science* (80- ). 228:1147-53.
- Gutiérrez S., Fernández-Novales J., Diago M.P., Tardaguila J. 2018. On-The-Go hyperspectral imaging under field conditions and machine learning for the classification of grapevine varieties. *Front. Plant Sci.* 9:1-11.
- Herrmann I., Shapira U., Kinast S., Karnieli A., Bonfil D.J., 2013. Ground-level hyperspectral imagery for detecting weeds in wheat fields. *Precis. Agric.* 14:637-59.
- Huang Y., Lee M.A., Thomson S.J., Reddy K.N. 2016. Ground-based hyperspectral remote sensing for weed management in crop production. *Int. J. Agric. Biol. Eng.* 9:98-109.
- Jay S., Gorretta N., Morel J., Maupas F., Bendoula R., Rabatel G., Dutartre D., Comar A., Baret F., 2017. Estimating leaf chlorophyll content in sugar beet canopies using millimeter- to centimeter-scale reflectance imagery. *Remote Sens. Environ.* 198:173-86.
- Jensen J.R. 2014. Remote sensing of the environment: an earth resource perspective, 2nd ed, Pearson Education Limited.
- Jiang Y., Li C., Robertson J.S., Sun S., Xu R., Paterson A.H. 2018. GPhenoVision: A ground mobile system with multi-modal imaging for field-based high throughput phenotyping of cotton. *Sci. Rep.* 8:1213.
- Liu D., Sun D.-W., Zeng X.-A. 2014. Recent advances in wavelength selection techniques for hyperspectral image processing in the food industry. *Food Bioprocess Technol.* 7:307-23.
- Liu D., Zeng X.A., Sun D.W. 2015. Recent developments and applications of hyperspectral imaging for quality evaluation of agricultural products: a review. *Crit. Rev. Food Sci. Nutr.* 55:1744-57.
- Lu R., Park B. 2015. Introduction. In: Park B., Lu R. (Eds), *Hyperspectral Imaging Technology in Food and Agriculture*. Springer, New York, NY, USA, pp. 3-7.
- Ma J., Sun D.-W., Pu H., Cheng J.-H., Wei Q. 2019. Advanced techniques for hyperspectral imaging in the food industry: principles and recent applications. *Annu. Rev. Food Sci. Technol.* 10:197-220.
- Malenovsky Z., Turnbull J.D., Lucieer A., Robinson S.A., 2015. Antarctic moss stress assessment based on chlorophyll content and leaf density retrieved from imaging spectroscopy data. *New Phytol.* 208:608-24.
- Mishra P., Asaari M.S.M., Herrero-Langreo A., Lohumi S., Diezma B., Scheunders P. 2017. Close range hyperspectral imaging of plants: A review. *Biosyst. Eng.* 164:49-67.
- Onoyama H., Ryu C., Suguri M., Iida M. 2018. Estimation of rice protein content before harvest using ground-based hyperspectral imaging and region of interest analysis. *Precis. Agric.* 19:721-34.
- Onoyama H., Ryu C., Suguri M., Iida M. 2015. Nitrogen prediction model of rice plant at panicle initiation stage using ground-based hyperspectral imaging: growing degree-days integrated model. *Precis. Agric.* 16:558-70.
- Pantazi X.E., Moshou D., Bravo C. 2016. Active learning system for weed species recognition based on hyperspectral sensing.

- Biosyst. Eng. 146:193-202.
- Reddy K.N., Huang Y., Lee M.A., Nandula V.K., Fletcher R.S., Thomson S.J., Zhao F. 2014. Glyphosate-resistant and glyphosate-susceptible Palmer amaranth (*Amaranthus palmeri* S. Wats.): Hyperspectral reflectance properties of plants and potential for classification. *Pest Manag. Sci.* 70:1910-7.
- Rinnan Å., Berg F., van den Engelsen S.B. 2009. Review of the most common pre-processing techniques for near-infrared spectra. *TrAC Trends Anal. Chem.* 28:1201-22.
- Rodríguez-Moreno F., Zemek F., Kren J., Píkl M., Lukas V., Novak J. 2016. Spectral monitoring of wheat canopy under uncontrolled conditions for decision making purposes. *Comput. Electron. Agric.* 125:81-8.
- Römer C., Wahabzada M., Ballvora A., Pinto F., Rossini M., Panigada C., Behmann J., Léon J., Thureau C., Bauckhage C., Kersting K., Rascher U., Plümer L. 2012. Early drought stress detection in cereals: simplex volume maximisation for hyperspectral image analysis. *Funct. Plant Biol.* 39:878-90.
- Thomas S., Kuska M.T., Bohnenkamp D., Brügger A., Alisaac E., Wahabzada M., Behmann J., Mahlein A.K. 2018. Benefits of hyperspectral imaging for plant disease detection and plant protection: a technical perspective. *J. Plant Dis. Prot.* 125:5-20.
- Underwood J., Wendel A., Schofield B., McMurray L., Kimber R. 2017. Efficient in-field plant phenomics for row-crops with an autonomous ground vehicle. *J. F. Robot.* 34:1061-83.
- Vigneau N., Ecartot M., Rabatel G., Roumet P. 2011. Potential of field hyperspectral imaging as a non destructive method to assess leaf nitrogen content in Wheat. *F. Crop. Res.* 122:25-31.
- Wang B., Zhang X., Dong Y., Zhang J., Zhang J., Zhou X. 2018. Retrieval of leaf chlorophyll content of paddy rice with extracted foliar hyperspectral imagery. pp 1-5 in 2018 7th International Conference on Agro-Geoinformatics (Agro-Geoinformatics), IEEE.
- Wendel A., Underwood J., Walsh K. 2018. Maturity estimation of mangoes using hyperspectral imaging from a ground based mobile platform. *Comput. Electron. Agric.* 155:298-313.
- Whetton R.L., Waine T.W., Mouazen A.M. 2018. Hyperspectral measurements of yellow rust and fusarium head blight in cereal crops: Part 2: On-line field measurement. *Biosyst. Eng.* 167:144-58.
- Wu Q., Wang C., Fang J.J., Ji J.W. 2016. Field monitoring of wheat seedling stage with hyperspectral imaging. *Int. J. Agric. Biol. Eng.* 9:143-8.
- Yoon S.-C., Park B. 2015. *Hyperspectral image processing methods*. Springer, New York, NY, pp. 81-101.
- Zhao J., Zhang D., Huang L., Zhang Q., Liu W., Yang H. 2016. Vertical features of yellow rust infestation on winter wheat using hyperspectral imaging measurements. pp 1-4 in 2016 5th Int. Conf. Agro-Geoinformatics.